A Model for Simultaneous Crystallisation and Biodegradation of Biodegradable Polymers

Xiaoxiao Han and Jingzhe Pan[1]

Department of Engineering, University of Leicester, Leicester, LE1 7RH, UK

[1] Corresponding author. Tel.: +44 116 223 1092; fax: +44 116 252 2525.
E-mail address: jp165@leicester.ac.uk

ABSTRACT: This paper completes the model of biodegradation for biodegradable polymers that was previously developed by Wang et al. (Wang Y, Pan J, Han X, Sinka, Ding L. A phenomenological model for the degradation of biodegradable polymers. Biomaterials 2008;29:3393-3401). Crystallisation during biodegradation was not considered in the previous work which is the topic of the current paper. For many commonly used biodegradable polymers, there is a strong interplay between crystallisation and hydrolysis reaction during biodegradation – the chain cleavage caused by the hydrolysis reaction provides an extra mobility for the polymer chains to crystallise and the resulting crystalline phase becomes more resistant to further hydrolysis reaction. This paper presents a complete theory to describe this interplay. The fundamental equations in the Avrami's theory for crystallisation are modified and coupled to the diffusion-reaction equations that were developed in our previous work. The mathematical equations are then applied to three biodegradable polymers for which long term degradation data are available in the literature. It is shown that the model can capture the behaviour of the major biodegradable polymers very well.

Keywords: Biodegradable polymers, biodegradation, crystallisation, modelling

Nomenclature

$\bar{A}$ non-dimensionalised form of *A* as defined in Eqs. (19) and (20)

C_e mole number of ester bounds of amorphous polymer per unit volume of *semi-crystalline polymer*

C_{e0} initial value of C_e

C_m mole number of monomers remained in the material per unit volume of *semi-crystalline polymer*,

D effective diffusion coefficient of monomers in degrading polymer

D_0 diffusion coefficient of monomers in amorphous polymer

D_{pore} diffusion coefficient of monomers in liquid-filled pores

G linear growth rate of a single crystal

N mole concentration of nuclei of crystallization

N_0 initial mole concentration of nuclei of crystallisation

R mole number of the amount of monomers produced by hydrolysis reaction per unit volume of *semi-crystalline polymers*.

V_{sing} volume of a single crystal

X_c volume degree of crystallinity

X_{ext} extended volume degree of crystallinity

$div_{x_i}\vec{\mathbf{X}}$ divergence of vector **X** in Cartesian coordinates x_i

$grad_{x_i}\vec{X}$ gradient of scale variable *X* in Cartesian coordinates x_i

c_e mole number of ester bounds of amorphous polymer per unit volume of the *amorphous polymer*

c_m mole number of monomers remained in the material per unit volume of *amorphous polymer*,

r mole number of the amount of monomers produced by hydrolysis reaction per unit volume of *amorphous polymer*,

k_1 reaction rate of non-catalyzed hydrolysis

k_2 reaction rate of auto-catalyzed hydrolysis

k_c Avrami constant for crystallisation

l characteristic length of device

n exponent of dissociation of acid end groups

m Avrami exponent

n_A Avogadro' number (= 6.02×10^{23})

p porosity of degrading polymer due to leaving monomers

r size of a single crystal

$r_{\max}$ maximum size of a single crystal

t degradation time

t_0 characteristic time of auto-catalyzed hydrolysis reaction ($t_0 = 1/k_2 C_{e0}^n$)

x_i *(i=1,2,3),* Cartesian coordinates

α shape factor of a single crystal ($4\pi/3$ for a sphere)

λ, η impingement parameter for crystallization, $\eta = 1/(\lambda - 1)$

τ life time of a single crystal

ξ probability of formation of growth nuclei per nucleus per unit time

1. Introduction

Linear aliphatic polyesters, poly(glycolide) (PGA), poly(lactide) (PLA) and their copolymers in particular, are being used in controlled drug delivery, orthopaedic fixation, tissue engineering and many other biomedical applications to provide various temporary functions inside human body [1]. The backbones of these polymers are highly hydrolysable and the degradation products are eventually metabolized into carbon dioxide and water. The devices "disappear" after serving their functions to let biology take over. Because of their well established biocompatibility, PGA, PLA and their copolymers are the most commonly used biodegradable polymers in medical devices. Sutures made of these polymers have been safely used since 1970. Biodegradable screws, plates and films are being increasingly used in orthopaedic fixations [2,3]. Drug delivery devices, temporary barriers for adhesion prevention and temporary vascular grafts are some other intensively investigated applications [4]. Currently the most pursued application is perhaps in tissue engineering to recreate or improve native tissue function using degradable scaffolds [5]. PGA, PLA and their copolymers are certainly not materials easy to work with. Among many other things, two complications have to be considered: (a) the biodegradation of polymers containing PLA is heterogeneous due to the autocatalytic nature of the hydrolysis reaction [6], and (b) many of these polymers, PGA and poly(L-lactide) (PLLA) for example, crystallise during biodegradation [7-9]. A complicated interplay between the hydrolysis reaction, diffusion of the reaction products and crystallisation makes the mechanical and functional properties of the biodegradable devices difficult to predict. So far the development of medical devices made of biodegradable polymers has been

almost entirely based on the trial and error approach. The lack of a mathematical framework for the biodegradation process makes it difficult to extrapolate experience and data obtained in one device to another. Because the biodegradation is dimension dependant, it is even difficult to extrapolate data between same devices of different dimensions (screws of different diameters for example). On the other hand, modern computer modelling techniques have been routinely used in engineering to optimise engineering designs. A close example is the design of engineering components operating at elevated temperatures, turbine blades in jet engines and hot steam pipes in power generation plants for examples. Alloys used in these applications experience microstructural "degradation" over a period of 10-30 years, reducing the strength of the components and limiting their service life. The methodology, especially the numerical techniques developed in the engineering design, can be readily applied to the design of biodegradable medical devices. However the underlying mechanism of polymer degradation is very different from that for the high temperature failure of engineering alloys. A mathematical framework is needed for the biodegradation process. In our previous paper, a set of simplified diffusion – reaction equations were established to model the biodegradation [10]. The model was compared with experimental data and a biodegradation map was presented showing the interplay between the hydrolysis reaction and the diffusion of the reaction products. The heterogeneous nature of the biodegradation was fully considered. However the interplay between crystallisation and biodegradation was not considered in the previous work. The current paper completes the model by incorporating

crystallisation into the diffusion-reaction equations. During biodegradation the chain scissions provide the extra mobility for the polymer chains to crystallise. The resulting crystalline phase becomes more resistant to further hydrolysis reaction. The crystallisation theory due to Avrami [11-13] has been shown to be valid for a wide range of materials including polymers. This theory predicts an exponential dependence of the degree of crystallinity on time. However the simple exponential equation cannot be directly applied to biodegradation because it does not consider the interaction between hydrolysis, diffusion and crystallisation. In this paper, we re-examine the fundamentals in the Avrami's theory and show that the theory can be modified and coupled to the diffusion-reaction equations to model simultaneous crystallisation and biodegradation. It is no longer possible to obtain analytical solutions to the resulting differential equations. Instead, these equations are solved numerically. The model is then applied to three different biodegradable polymers including poly(glycolide-co-L-lactide), poly(L-lactide), and blends of poly(L-lactide) and poly(vinyl alcohol), for which complete biodegradation data are available in the literature [3-5]. Finally parametric studies are carried out using the model to demonstrate the effects of crystallisation rate on the degradation rate and on the biodegradation map.

2. Governing equations for simultaneous crystallisation and biodegradation

It has been widely observed that the degree of crystallinity in commonly used biodegradable polymers increases significantly during both short term and long term

degradation [7-9]. The degradation-induced crystallisation can occur in either initially amorphous or semi-crystalline polymers. Important examples of the biodegradable polymers are PGA, PLLA and their copolymers. PGA is a highly crystalline polymer while PLLA is semi-crystalline. The crystalline phase provides these polymers with the necessary mechanical strength for the medical devices. During biodegradation, the hydrolysis reaction of the ester backbone in aqueous environment leads to cleavage of the polymer chains and produces short oligomers. The oligomers then diffuse out of the material leading to a weight loss of the device. For a semi-crystalline polymer, the chain cleavage occurs preferentially in the amorphous region. Therefore even if the total volume of the crystalline phase remains constant, the observed degree of crystallinity still increases due to the loss of the amorphous phase. More importantly, cleavage of the long and amorphous polymer chains provides higher mobility for the polymer chains, facilitating the crystallisation of the amorphous polymer [7]. The detailed degradation pathways have been suggested [7] and long term experimental data of simultaneous degradation and crystallisation are available in the literature [8,9]. However a mathematical model for the degradation-induced crystallisation does not exist as far as the authors are aware. Avrami's theory [11-13] has been shown to be generally valid for polymer crystallisation [14]. It predicts that the degree of crystallinity, X_c depends on time, *t*, in an exponential manner:

$$X_c = 1 - \exp -(k_c t)^m \quad (1)$$

in which *m* is a constant often referred to as the Avrami exponent and k_c is a temperature dependent factor (often taken as an Arrhenius type expression). This

equation however does not taken into account of the interaction between polymer chain cleavage and crystallisation, and therefore cannot be directly applied to biodegradation. However it is possible to modify Avrami's differential equations [11-13] led to Eq. (1) to model the degradation-induced crystallisation.

Following our previous work [10], a biodegradable polymer can be viewed as being consisted of four species:

I. amorphous polymer molecules, which can hydrolyse but are too large to diffuse; part of the polymer molecules can also crystallise;

II. monomers, which are the product of the hydrolysis reaction and can diffuse;

III. polymer crystals, which are formed and grow but do not hydrolyse.

IV. water molecules, which are assumed to be abundant anywhere in the device;

The state of a biodegrading polymer can therefore be completely described using

a) C_e - mole number of ester bounds of amorphous polymer per unit volume of *semi-crystalline polymer*,

b) C_m - mole number of monomers remained in the material per unit volume of *semi-crystalline polymer*, and

c) X_c - the volume degree of crystallinity.

It is assumed that the hydrolysis reaction only occurs in the amorphous region despite that the ester groups of polymer chains on the surface of the crystalline region are hydrolyzed. It is then necessary to further define the following variables:

d) c_e - mole number of ester bounds of amorphous polymer per unit volume of the *amorphous polymer*,

e) c_m - mole number of monomers remained in the material per unit volume of *amorphous polymer*,

f) r - mole number of the amount of monomers produced by hydrolysis reaction per unit volume of *amorphous polymer*.

The production rate of monomers by the hydrolysis reaction is given by [15]

$$\frac{dr}{dt} = k_1 c_e + k_2 c_e c_m^n \tag{2}$$

in which k_1 and k_2 are the reaction constants for the non-autocatalytic and autocatalytic hydrolysis reactions. The power n in the second term accounts for the dissociation of the acid end groups. The mole concentrations in the amorphous phase and those in the semi-crystalline polymer are connected by

$$c_e = \frac{C_e}{1-X_c}; \quad c_m = \frac{C_m}{1-X_c}. \tag{3}$$

Using Eq. (3) in Eq. (2) gives

$$\frac{dr}{dt} = \frac{1}{1-X_c}\left\{k_1 C_e + k_2 \frac{C_e C_m^n}{(1-X_c)^{n-1}}\right\}. \tag{4}$$

It turns out to be convenient to defining a new variable R using

$$\frac{dR}{dt} = (1-X_c)\frac{dr}{dt} = k_1 C_e + k_2 \frac{C_e C_m^n}{(1-X_c)^{n-1}}. \tag{5}$$

R represents the moles of monomers produced per unit volume of the semi-crystalline polymer. It also reflects the total number of chain cleavages per unit volume of the semi-crystalline polymer. The reduction in the ester bound concentration in the amorphous phase originates from two parts: (a) hydrolysis of the polymer chains and (b) crystallisation of the mobile polymer chains, which can be expressed as

$$\frac{dC_e}{dt} = -\frac{dR}{dt} - \frac{C_e}{1-X_c}\frac{dX_c}{dt}. \tag{6}$$

The second term on the left hand side in Eq. (6) represents the lost of amorphous polymer phase due to crystallisation.

Assuming Fick's law for monomer diffusion, we have the following governing equation for the monomer concentration:

$$\frac{dC_m}{dt} = \frac{dR}{dt} + \underset{x_i}{div}\left(D \underset{x_i}{grad} C_m \right) \tag{7}$$

in which D is the phenomenological diffusion coefficient. The nomenclature of vector analysis is used to shorten the expression of Eq. (6). The effective diffusion coefficient D of the degrading polymer is a function of the porosity, p, and degree of crystallinity, X_c. In our previous paper [10] a linear relation between D and p was assumed, which is valid if the porosity is less than 25%. To improve the linear approximation, finite element calculations of the effective diffusion coefficient were carried out using a three dimensional representative cubic material. A randomly distributed second phase was gradually introduced into the unit and the effective diffusion coefficient of the two phase material was calculated numerically. Details of the analysis will be published elsewhere [16]. The conclusion of the numerical study is that the numerical results can be fitted into the following empirical equation:

$$D = D_{slow} + 1.3V_{fast} - 0.3V_{fast}^2 - 0.3V_{fast}^3 \left(D_{fast} - D_{slow} \right) \tag{8}$$

in which D_{slow} and D_{fast} represent the diffusion coefficients of the fast and slow diffusion phases respectively and V_{fast} represents the volume fraction of the fast diffusion phase. Eq. (8) is valid if $D_{fast}/D_{slow} > 10$. For a degrading polymer

containing pores which are generated by monomers diffusing out, its effective diffusion coefficient can be calculated using Eq. (8) as

$$D = D_{matrix} + \left(1.3p^2 - 0.3p^3\right)\left(D_{pore} - D_{matrix}\right), \tag{9}$$

in which D_{matrix} and D_{pore} represent the diffusion coefficients of monomers in the polymer matrix and pores respectively. The porosity *p* can be estimated as

$$p = 1 - \left(\overline{C}_m + \overline{C}_e\right)\left(1 - X_{c0} + X_c\right), \tag{10}$$

in which $\overline{C}_e = C_e / C_{e0}$ and $\overline{C}_m = C_m / C_{e0}$ where $C_{e0} = C_e\,(t = 0)$; X_{c0} is the initial degree of crystallinity. The polymer matrix is consisted of an amorphous and a crystalline phase. It can be assumed that the diffusion coefficient of the monomers in the crystalline phase is zero (D_{slow} = 0). Using D_0 to represent the diffusion coefficient of monomers in the amorphous polymer, the effective diffusion coefficient of the polymer matrix can be obtained from Eq. (8) as

$$D_{matrix} = \left[1.3\left(\frac{\overline{C}_m + \overline{C}_e}{\overline{C}_m + \overline{C}_e + X_c/(1 - X_{c0})}\right)^2 - 0.3\left(\frac{\overline{C}_m + \overline{C}_e}{\overline{C}_m + \overline{C}_e + X_c/(1 - X_{c0})}\right)^3\right] D_0 \tag{11}$$

The effective diffusion coefficient of the degrading polymer can be determined by combining Eqs (9-11).

The centre piece of Avrami's theory [11-13] is the relation between the volume degree of crystallinity, X_c, and a so-called extended volume fraction of the crystalline phase, X_{ext} which is given by

$$\frac{dX_c}{dX_{ext}} = 1 - X_c. \tag{12}$$

The extended volume is a fictitious volume of the crystals imagining that the crystal growth is unimpeded by impingement upon each other. X_{ext} is therefore much easier

to calculate than X_c. The Avrami's expression of Eq. (1) was directly derived from Eq. (12). In this study, it was quickly realized that Avrami's theory based on Eq. (12) is unable to capture the observed crystallisation behavior in biodegradable polymers. The first problem is that Eq. (12) always predicts to a significant incubation period for crystallisation which is very short during biodegradation [7-9]. The second problem is that Eq. (12) always predicts full crystallisation as time approaches infinity which is not true for most biodegradable polymers. The following modification to Eq. (12) is used to overcome these problems:

$$\frac{dX_c}{dX_{ext}} = 1 - X_c \quad . \tag{13}$$

Here λ, or its another form, $\eta = 1/(\lambda - 1)$, is referred to as the impingement parameter in the literature, which was introduced by previous researchers to provide a better fit with experimental data [17].

The next fundamental element in Avrami's theory is the governing equation for the crystallisation nuclei. In Avrami's theory, it is assumed that there exist a fixed number of nuclei at the beginning of the crystallisation and that they are gradually used up as the crystallisation continues. Using *N* to represent the mole concentration of the nuclei at time *t*, Avrami proposed the following equation [11-13]:

$$dN = -\xi N dt - \frac{N}{1 - X_c} dX_c \, . \tag{14}$$

The first term on the left hand side represents the number of nuclei that become active growth during time interval *dt* in consequence of free energy fluctuation. ξN represents the probability of this happening. The second term represents the number

of nuclei that are swallowed by the growing crystals. Eq. (14) is subject to the initial condition that $N = N_0$ at $t = 0$. During cleavage-induced crystalisation, the amorphous polymer chains only start to crystallise where chain cleavage occurs, i.e. a nucleus (a foreign inclusion for example) can only become available if a chain cleavage occurs nearby. In a small time interval of *dt*, the increase in chain cleavage is quantified by *dR* given by Eq. (5). Keeping in mind that that N_0 and C_{e0} represent the initial concentrations of the nuclei and the ester bounds respectively, we propose to modify Eq. (14) as

$$dN = -\xi N dt - \frac{N}{1 - X_c} dX_c + \frac{N_0}{C_{e0}} dR, \tag{15}$$

subject to the initial condition that $N = 0$ at $t = 0$. The newly added term on the right hand side represents the nuclei released by chain cleavage over time interval of *dt*. In Eq. (15), *N* is the number of nuclei that are made available by polymer chain cleavage. *N* increases from zero to a maximum number and then decreases as crystallisation continues.

Following Avrami [11-13] the extended volume fraction of the crystals, X_{ext}, can be calculated as

$$X_{ext} = \int_0^t V_{sing}(t - \tau)\, \xi N(\tau)\, n_A\, d\tau \tag{16}$$

in which n_A is the Avogadro's number (6.02×10^{23}) and $V_{sing}(t - \tau)$ is the volume of a single crystal at time *t* that is nucleated at time τ. Avrami's theory assumes linear growth for a single crystal. For polymers the crystal grows through chain folding which is constrained by the entropic frustration of the participating polymer chains [18]. Consequently the crystallised lamellae can only reach a limited size,

which is referred to as $r_{\max}$. In this paper, the linear growth limited by a maximum size is approximated by the following function:

$$r = r_{\max}\left(1 - e^{-\frac{G}{r_{\max}}(t-\tau)}\right) \tag{17}$$

in which *G* is the linear growth rate. We then have $V_{sing}(t-\tau) = \alpha r^3$ and Eq. (16) becomes

$$X_{ext} = \int_0^t \alpha r_{\max}^3 \left(1 - e^{-\frac{G}{r_{\max}}(t-\tau)}\right)^3 \xi N(\tau) n_A d\tau \tag{18}$$

in which α is a numerical constant depending on the shape of the crystal.

As demonstrated in our previous paper [10], it is constructive to use the non-dimensional form of the governing equations. The following non-dimensional variables are introduced:

$$\bar{C}_e = \frac{C_e}{C_{e0}};\ \bar{C}_m = \frac{C_m}{C_{e0}};\ \bar{R} = \frac{R}{C_{e0}};\ \bar{N} = \frac{N}{C_{e0}};\ \bar{x}_i = \frac{x_i}{l};\ \bar{t} = \frac{t}{(1/k_2 C_{e0}^n)} = \frac{t}{t_0} \tag{19}$$

together with the following non-dimensionalised parameters in the model:

$$\bar{D}_0 = \frac{D_0}{k_2 l^2 C_{e0}^n};\ \bar{k}_1 = \frac{k_1}{k_2 C_{e0}^n};\ \bar{N}_0 = \frac{N_0}{C_{e0}};\ \bar{r}_{\max} = \alpha C_{e0} n_A r_{\max}^3;\ \bar{G} = \frac{t_0 G}{r_{\max}};\ \bar{\xi} = t_0 \xi. \tag{20}$$

Here C_{e0} is the mole concentration of the amorphous ester bounds at the beginning of biodegradation and *l* is a characteristic length of device. The governing equations then become

$$\frac{d\bar{R}}{d\bar{t}} = \bar{k}_1 \bar{C}_e + \bar{C}_e \left(\frac{\bar{C}_m}{1 - X_c}\right)^n; \tag{21}$$

$$\frac{d\bar{C}_m}{d\bar{t}} = \frac{d\bar{R}}{d\bar{t}} + div_{\bar{x}_i}\left(\bar{D}\, grad_{\bar{x}_i} \bar{C}_m\right); \tag{22}$$

$$\frac{d\bar{C}_e}{d\bar{t}} = -\frac{d\bar{R}}{d\bar{t}} - \frac{\bar{C}_e}{1 - X_c}\frac{dX_c}{d\bar{t}}; \tag{23}$$

$$\frac{dX_c}{dX_{ext}} = 1 - X_c \quad ; \tag{24}$$

$$d\bar{N} = -\bar{\xi}\bar{N}d\bar{t} - \frac{\bar{N}}{1-X_c}dX_c + \bar{N}_0 d\bar{R} \; ; \tag{25}$$

$$X_{ext} = \bar{r}_{\max}\bar{\xi}\int_0^{\bar{t}} \left(1 - e^{-\bar{G}\left(\bar{t}-\bar{\tau}\right)^3}\right)\bar{N}\, d\bar{\tau} \; . \tag{26}$$

Eqs. (21-26) form the governing equations for simultaneous biodegradation and crystallisation. Eqs. (21-23) govern the biodegradation while Eqs. (24-26) govern the crystallisation. The last term in Eq. (23) connects biodegradation with crystallisation in the simple sense that crystallisation reduces the concentration of the amorphous polymers. The last term in Eq. (25) connects crystallisation with biodegradation in the simple sense that an existing nucleus can only become available for crystallisation if a chain cleavage occurs nearby. It is useful to point out the following issues when comparing the model predictions with experimental data:

a) As biodegradation approaches its end, most of the amorphous polymer chains are exhausted and the validity of Eqs. (15) and (17) become questionable. We are however less interested in the last part of the degradation as a device would have broken apart by then.

b) For simplicity the molecular weight distribution of the amorphous polymer chains has been simplified into a bimodal distribution, which is characterised by C_e and C_m. Assuming the monomers are too small to detect using standard experimental techniques, the measured average molecular weight M can be related to C_e such that $M/M_0 = C_e/C_{e0}$ in which M_0 and C_{e0} are the initial values of the average molecular weight and ester bound

concentration respectively. The model does not distinguish between number averaged and weight averaged molecular weights, which is a shortcoming of the simplification. One needs to choose one of the averaged molecular weights. The parameters in the model, k_1 and k_2, are then defined accordingly.

c) The volume degree of crystallinity, X_c, does not include the effect of weight-loss which has to be considered when comparing with experimental data. The observed degree of crystallinity is given by, $X_{obs} = X_c/(1-W)$, in which *W* represents the weight-loss in percentage which can be calculated from knowing the monomers diffusing out of the material.

3. Model validation

A computer programme is developed to solve the equations (21-26) numerically for infinitively large plate of thickness *2l*. At the surface of the plate, it is assumed that any monomer arriving at the surface is immediately taken away by the aqueous medium. The numerical details are not discussed here in order to focus on the physics of the model. However to demonstrate the robustness of the numerical procedure and to check the computer code, the numerical model is reduced to Avrami's theory by switching off biodegradation and diffusion. A initial value, N_0, was set for the number of nuclei and a very large value was used for $r_{\max}$. Analytical solutions to Avrami's theory are given by [11-13]

$$X_c = 1 - e^{-\alpha N_0 G^3 t^3}, \tag{27}$$

for large ξ, and by

$$X_c = 1 - e^{-\alpha N_0 \xi G^3 t^4 / 4}, \tag{28}$$

for small ξ. Fig. 1 shows the comparison between the numerical and analytical solutions. It can be seen from the figure that our model can be successfully reduced to the Avrami's theory. The degradation and diffusion parts of the numerical model have been validated in our previous work against finite element solution obtained using a commercial package [10].

Tsuji and his co-workers carried out a series of long term biodegradation experiments and published complete sets of data of average molecular weights, weight loss, degree of crystallinity and mechanical properties as functions of time for a range of PLA and its copolymers. The first case that we examined here is their experiment on pure PLLA and two blends of PLLA and poly(vinyl alcohol) (PVA) [8]. The degradation data were collected over a period of 12 months. PVA was introduced as a hydrophilic water-insoluble polymer to accelerate the biodegradation. In the blend films, PLLA and PVA were phase-separated and both the PLLA and PVA phases were continuous and dispersed. The two blends have weight percentages of PLLA of 80% and 60% respectively. In all the films the PLLA phase was initially amorphous while the PVA phase was semi-crystalline. The introduction of PVA complicates the degradation behavior, hence provides a test for the flexibility of the mathematical framework proposed in this paper. To take account of the PVA phase in the model, Eqs. (21)-(23) are modified to ensure that hydrolysis reaction only occurs in the amorphous region of the PLLA. This is achieved by adding the volume fraction of PVA to X_c in Eqs. (21) and (23). The crystalline phase of the PVA was excluded

as well as the crystalline phase in the PLLA when calculating the effective diffusion coefficient. Fig. 2 shows the fitting between the model and the experimental data for weight percentage of PLLA of 100% (Fig. 2(a)), 80% (Fig. 2(b)) and 60% (Fig. 2(c)) respectively. Table one shows the parameters used in the model to fit the experimental data which will be discussed together with other cases at the end of this section.

The second case that we studied is their experiment on pure PLLA films with different degrees of initial crystallinity [9], which were achieved by annealing the PLLA films at different temperatures. The experimental data were collected over a period of 36 months. The actual morphology of the semi-crystalline PLLA is complicated. There are different dimensional and spacing parameters of the crystalline lamellae as well as the size of the crystalline spherulites. There are also amorphous phase inside and outside the crystalline spherulites. All these structural details are ignored in our model and the degree of crystallinity is the only parameter used to describe the crystalline phase. This case, therefore, provides a test for the simplification in the model. Fig. 3 shows the fitting between the model and the experimental data for PLLA with initial degree of crystllinity of 40% (Fig. 3(a)), 47% (Fig. 3(b)), and 54% (Fig. 3(c)) respectively. Table one shows the parameters used in the model in order to fit the experimental data. The third case that we examined is the poly(glycolide-*co*-L-lactide) studied by Zong et al. [7]. Fig. 4 shows the fitting between the model and the experimental data. Again the parameters used in the model are given in Table one. This is a fast degradation case which took just two weeks to complete. Similar to the second case, the crystalline morphology experienced a

sophisticated evolution as clearly explained by Zong et al. [5].

It can be observed from Figs. 2-4 that the model fits with all the experimental data very well except for the last data points where the model is invalid. During the biodegradation, the crystallisation, hydrolysis reaction and diffusion of the hydrolysis are highly interconnected. The crystallisation reduces the region where the hydrolysis reaction operates, the hydrolysis reaction encourages further crystallisation and the diffusion process retards the auto-catalytic hydrolysis reaction and leads to weight-loss. Figs 2-4 show that the model developed in this paper can capture this sophisticated interplay for three vary different biodegradable polymers. The material parameters obtained for the three biodegradable polymers are presented together in Table one so that they can be examined together. The parameters are presented in the non-dimensional form for an easy comparison between the different materials. As will be seen in the following section of this paper, four of the crystallisation parameters, including $\overline{N}_0$, $\bar{r}_{\max}$, $\overline{G}$ and $\bar{\xi}$, affect the crystallisation rate as a group. We therefore fixed $\overline{N}_0$, $\bar{r}_{\max}$, and $\bar{\xi}$ for all the materials and only varied $\overline{G}$. $\overline{N}_0 = 1$ means that we have assumed each chain cleavage gives a new nucleation site; Using $C_{e0} = 17300\, mole/m^3$ for PLLA and $n_A = 6.02\times10^{23}$, $\bar{r}_{\max} = 4\pi/3\times10^5$ corresponds to a maximum size of the polymer crystals of 20*nm*; $\bar{\xi} = 1000$ corresponds to the upper limit of $\bar{\xi}$ in the original Avrami's theory. $\overline{G} = 1$ corresponds to a growth rate at which a crystal reaches its maximum size of $r_{\max}$ at $t = t_0$. The values of $\overline{G}$ in Table one correspond to rather slow growth but this is because the large values of $\overline{N}_0$ and $\bar{\xi}$ used in the model. The impingement factor, η, is a fitting parameter in

the model which has a profound impact on the crystallisation behavior. It will be further discussed in the following section of this paper. The intrinsic diffusion coefficient, $\overline{D}_0$, was mainly determined by the weight-loss. $\bar{k}_1$ and t_0 are mainly determined by the reduction rate of the average molecular weight. $\overline{D}_0$, $\bar{k}_1$ and t_0 can therefore be regarded as being measured through the model and the experiments.

4. The interplay between degradation and crystallisation

It is useful to study what the model predicts in terms of the effect of crystallisation rate on the apparent hydrolysis rate of the material. The apparent hydrolysis rate can be characterised using the time required for $\overline{C}_e$ to reach a fix value, say 0.5. The crystallisation rate can then be characterised using the corresponding value of $X_c - X_{c0}$ at $\overline{C}_e = 0.5$. However there are five parameters in the crystallisation model, including $\overline{N}_0$, $\bar{r}_{\max}$, $\overline{G}$, $\bar{\xi}$, and η, which all affect the crystallisation rate. Fig. 5 shows the calculated degrees of crystallinity as a function of time using a wide range of values of the five parameters which all give $X_c = 0.2$ at $\overline{C}_e = 0.5$. It can be clearly seen from the figure that if the impingement factor η is fixed, then X_c at a fix value of $\overline{C}_e$ almost completely determines the crystallisation behavior. In other words, $\overline{N}_0$, $\bar{r}_{\max}$, $\overline{G}$, and $\bar{\xi}$, act as a group to control the crystallisation rate. The impingement factor, however, has an independent effect on the crystallisation behavior which cannot be accommodated into the group. Fig. 6 shows the effect of crystallisation rate on the hydrolysis rate. The model predicts that fast crystallisation leads to fast apparent hydrolysis in the amorphous phase. It is often said

in the literature that fast crystallisation retards biodegradation. This is obvious because the crystalline phase resists further hydrolysis reaction. However Tsuji and Ikada [9] carefully distinguished this from the effect of crystallisation on the hydrolysis rate in the amorphous region and observed that the hydrolysis rate was higher in the amorphous region between the crystalline regions than that of the free amorphous region such as in a completely amorphous specimen. Our model prediction is therefore consistent with the experimental observation by Tsuji and Ikada [9]. It is interesting to observe from Fig. 6 that the effect of crystallisation on the hydrolysis is almost independent of $\bar{k}_1$, the relative rate between the non-catalyzed and auto-catalyzed reactions.

An important concept proposed in our previous work [10] is the biodegradation map which shows the controlling mechanism for biodegradation in the landscape of $\bar{D}_0$ and $\bar{k}_1$. The map for infinitively large plate is presented in Fig 7 where the dash lines shows the boundaries between the different zones for amorphous polymers. We recall that zone *B* is the fast diffusion zone where the polymer degradation is controlled by the non-catalysed hydrolysis. Zone *C* is the slow diffusion zone where the degradation is controlled by the auto-catalysed hydrolysis. Zone *D* is the fast non-catalysed hydrolysis zone and zone *A* is where hydrolysis and diffusion interact to control the degradation rate. Under the assumption of fast water penetration into the device, biodegradation is spatially uniform except in zone A. The shaded region on the map is the newly calculated zone A for $X_C =$ 0.7 to 0.8 at $\bar{C}_e$ = 0.3 to 0.4. These values reflect a fast crystallisation rate in the biodegradation. The ranges in these

values are used because it is difficult to construct the map and control the values of X_c and $\overline{C}_e$ at the same time. The impingement factor was set as $\eta = 0.5$. Fig. 7 shows that crystallisation makes it more likely for the biodegradation to be spatially uniform. Most of the biodegradation experiments were performed using thin samples to avoid the accumulation of acid end groups inside the film, i.e. to operate in zone *B*. The map in Fig. 7 shows that one can use thicker samples for semi-crystallized polymers than those for amorphous polymers, which should make the following mechanical tests easier.

5. Concluding remarks

The typical degradation time for commonly used biodegradable polymers in orthopaedic surgeries can be several years. The trial and error approach in device development is very problematic. The mathematical model developed in the paper can be solved for any sophisticated device using the modern finite element method [10]. Many experience and degradation data have been collected for various existing devices. It is then possible to use the finite element analysis to back-calculated the parameters in the model and to apply them to new device design using the same polymers. This is a powerful approach which will accelerate the development of various biodegradable devices.

Acknowledgements: Xiaoxiao Han gratefully acknowledges a partial PhD studentship from an EPSRC research grant (S57996).

References

[1] Sodergard A, Stolt M. Properties of lactic acid based polymers and their correlation with composition. Progress in Polymer Science 2002;27:1123-1163.

[2] Wood GD. Inion biodegradable plates: the first century. British Journal of Oral and Maxillofacial Surgery 2006;44:38-41.

[3] Bell RB, Kindsfater CS. The Use of Biodegradable Plates and Screws to Stabilize Facial Fractures. Journal of Oral and Maxillofacial Surgery 2006;64:31-39.

[4] Siepmann J, Siepmann F, Florence AT. Local controlled drug delivery to the brain: mathematical modeling of the underlying mass transport mechanisms. International Journal of Pharmaceutics 2006;314:101-119.

[5] Sengers BG, Taylor M, Please CP, Oreffo ROC. Computational modeling of cell spreading and tissue regeneration in porous scaffolds. Biomaterials 2007; 28: 1926-1940.

[6] Grizzi I, Garreau H, Li S and Vert M. Hydrolytic degradation of devices based on poly[DL-lactic acid] size dependence**.** Biomaterials 1995;16:305-311.

[7] Zong XH, Wang ZG, Hsiao BS, Chu B, Zhou JJ, Jamiolkowski DD, et al. Structure and morphology changes in absorbable poly(glycolide) and poly(glycolide-co-lactide) during in vitro degradation. Macromolecules 1999;32:8107–14.

[8] Tsuji H, Muramatsu H. Blends of aliphatic polyesters: V Non-enzymatic and enzymatic hydrolysis of blends from hydrophobic poly(L-lactide) and hydrophilic poly(vinyl alcohol). Polymer Degradation and Stability 2001;71:403-413.

[9] Tsuji H, Ikada Y. Properties and morphology of poly(L-lactide) 4: effects of structural parameters on long-term hydrolysis of poly(L-lactide) in phosphate-buffered solution. Polymer Degradation and Stability 2000;67:179–89.

[10] Wang Y, Pan J, Han X, Sinka IC, Ding L. A phenomenological model for the degradation of biodegradable polymers. Biomaterials 2008;29:3393-3401.

[11] Avrami M. Kinetics of phase change I: general theory. Journal of Chemical Physics 1939;7:1103–12.

[12] Avrami M. Kinetics of phase change II: transformation-time relations for random distribution of Nuclei. Journal of Chemical Physics 1940;8:212–24.

[13] Avrami M. Kinetics of phase change III: granulation, phase change, and microstructure. Journal of Chemical Physics 1941;9:177–84.

[14] Long YU, Shanks RA, Stachurski ZH. Kinetics of Polymer Crystallisation. Prog. Polym. Sci. 1995;20:651-701.

[15] Siparsky GL, Voorhees KJ, Miao F. Hydrolysis of polylactic acid (PLA) and polycaprolactone (PCL) in aqueous acetonitrile solutions: autocatalysis. Journal of Environmental Polymer Degradation 1998;6:31-41.

[16] Jiang WG, Han X, Pan J. Effective diffusion coefficient of biodegradation polymers and its role in degradation. University of Leicester Research Report 2008.

[17] Starink MJ. On the meaning of the impingement parameter in kinetic equations for nucleation and reaction reactions. Journal of Materials Science. 2001; 36:4433-4441.

[18] Muthukumar M. Molecular modelling of nucleation in polymers. Phil. Trans. R. Soc. Lond. A. 2003;361:539-556.

Table one – Parameters used in the model to fit the experimental data for the different cases.

Parameters / Materials		$\overline{D}_0$	$\overline{k}_1$	$\overline{N}_0$	$\overline{r}_{\max}$	$\overline{G}$	$\overline{\xi}$	η	t_0 (week)
PLLA/PVA	V_{PLLA}=100%	0.002	2	1	$4\pi/3\times10^5$	0.05	1000	0.015	94.54
	V_{PLLA}=80%	0.0005	2	1	$4\pi/3\times10^5$	0.1	1000	0.015	49.52
	V_{PLLA}=60%	0.005	2	1	$4\pi/3\times10^5$	1	1000	0.015	40.8
PLLA	X_{c0}=0.4	0.002	1	1	$4\pi/3\times10^5$	0.3	1000	0.08	109.1
	X_{c0}=0.47	0.02	1	1	$4\pi/3\times10^5$	0.7	1000	0.08	94.23
	X_{c0}=0.54	0.02	5	1	$4\pi/3\times10^5$	1	1000	0.125	312
PLA-*co*-PGA		1	2	1	$4\pi/3\times10^5$	2	1000	0.1	14.29

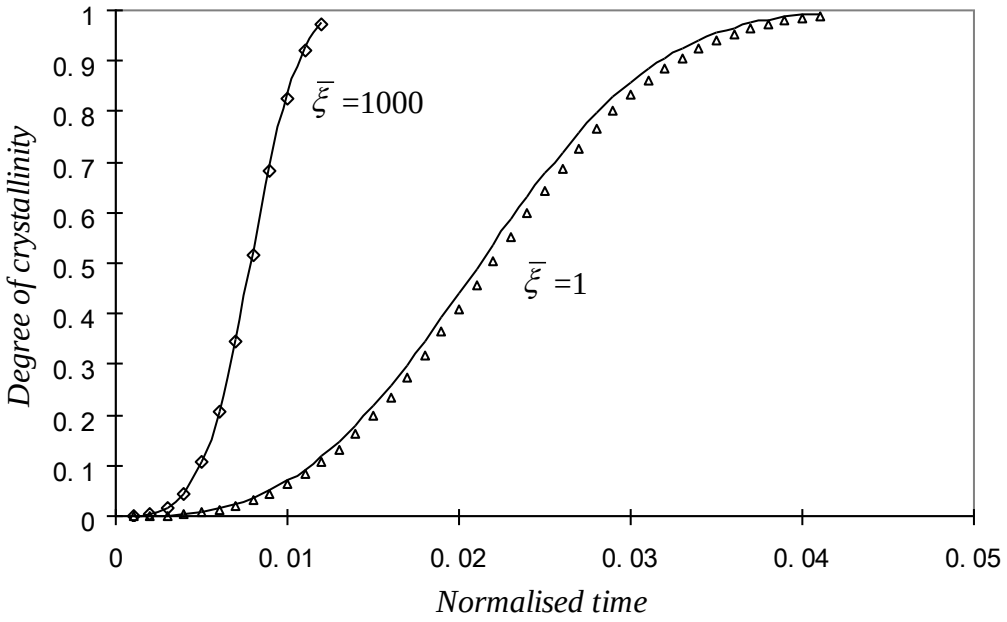

Fig. 1. Degree of crystallinity as a function of time for large and small values of $\bar{\xi}$ - a comparison between the analytical solutions of the Avrami's theory (solid lines) and the numerical solutions (discrete symbols) of the simultaneous degradation and crystallisation model when it is reduced to the Avrami's theory. $\bar{N}_0 = 1;\ \bar{G} = 1;$ $\lambda = 1;\ \bar{r}_{\max} = 4\pi / 3 \times 10^8.$

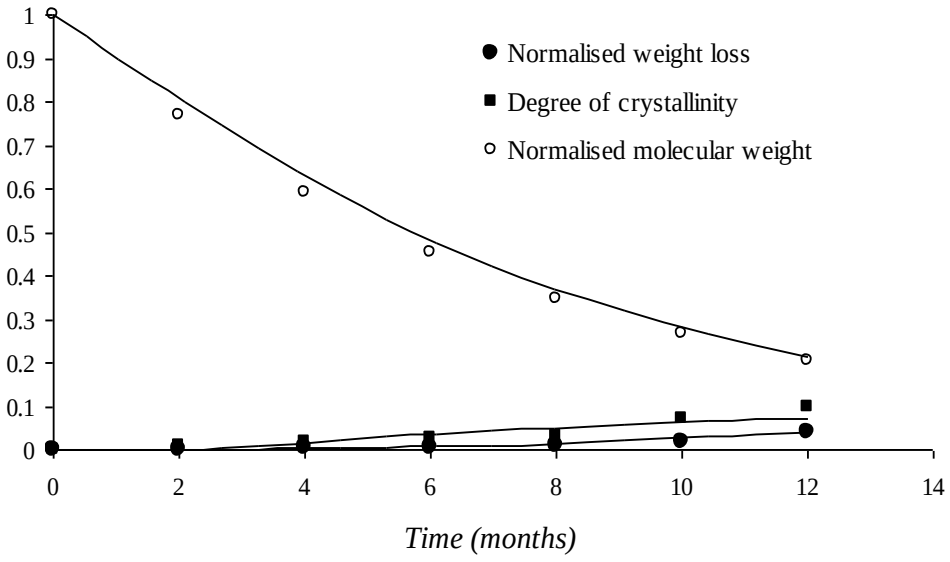

(a) 100% PLLA

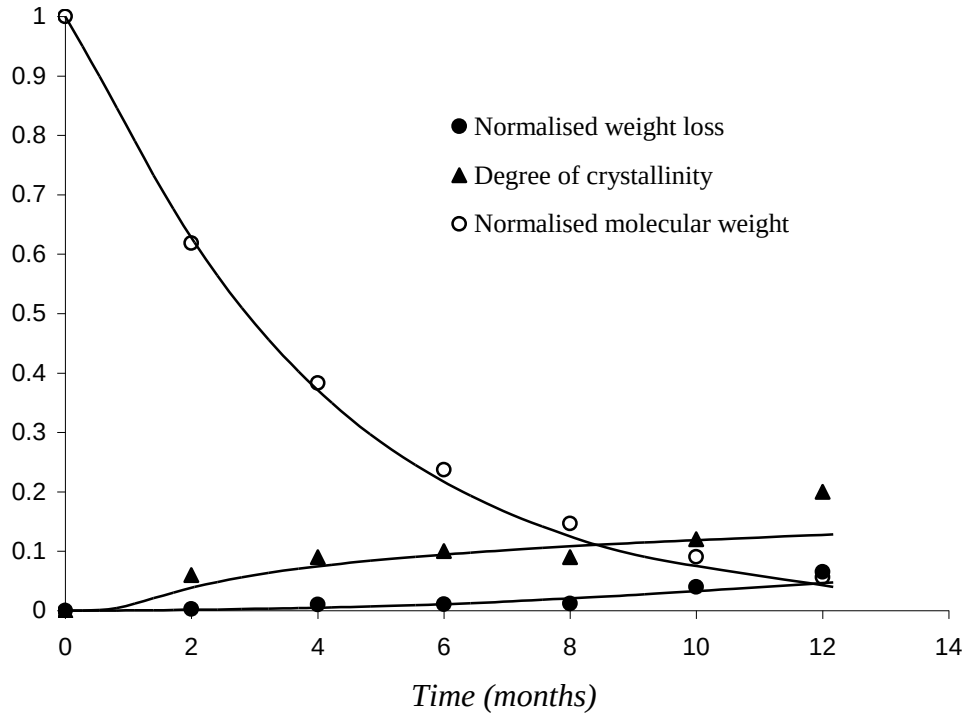

(b) 80% PLLA

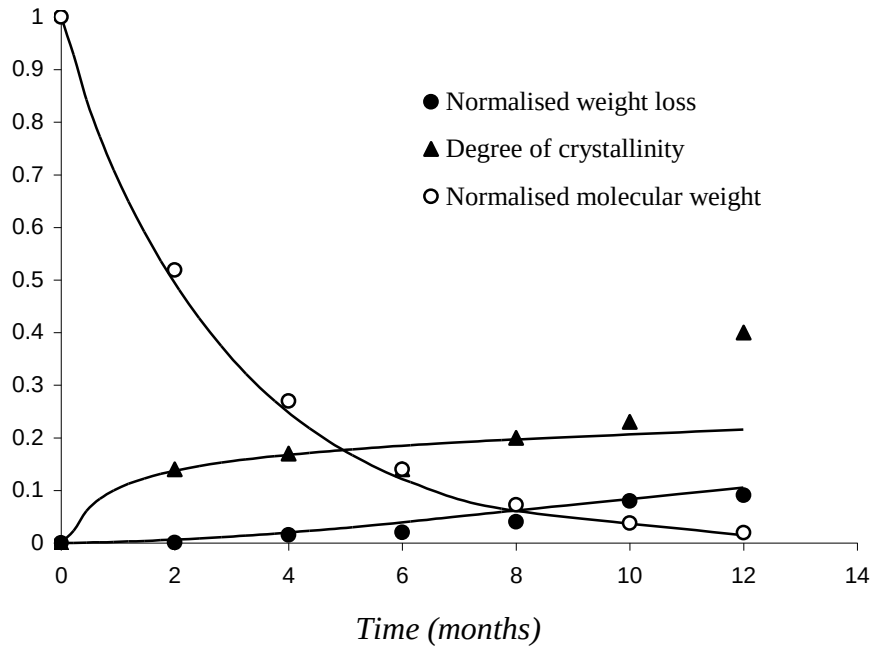

(c) 60% PLLA

Fig. 2. Comparison between the model and the experimental data obtained by Tsuji and Muramatsu [8] for average molecular weight of PLLA, volume degree of crystallinity of PLLA and weight loss of the film as functions of time for volume percentage of PLLA = 100% (a), 80% (b) and 60% (c) respectively. The continuous lines represent the model prediction while the discrete symbols are the experimental data. The parameters used in the model are given in Table 1.

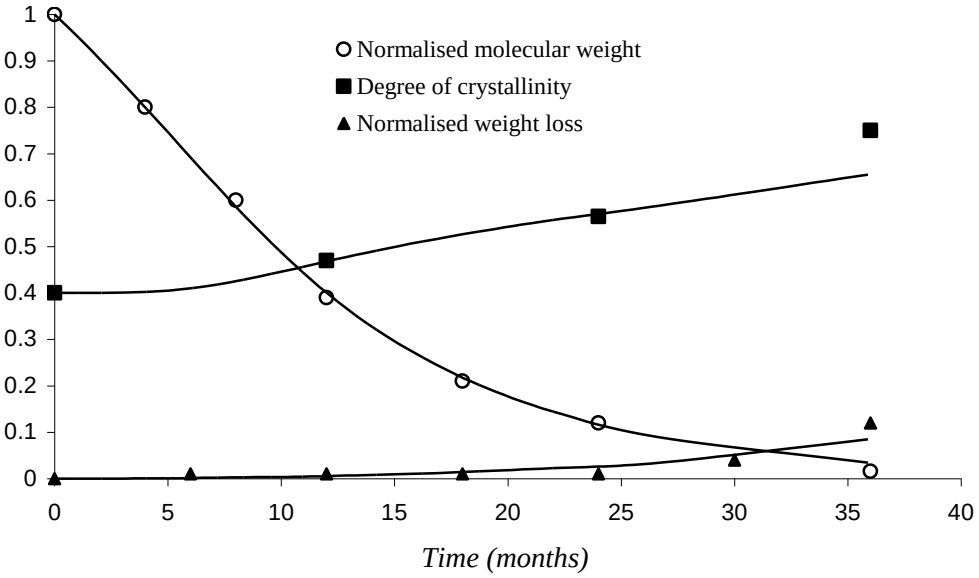

(a) $X_{c0} = 40\%$

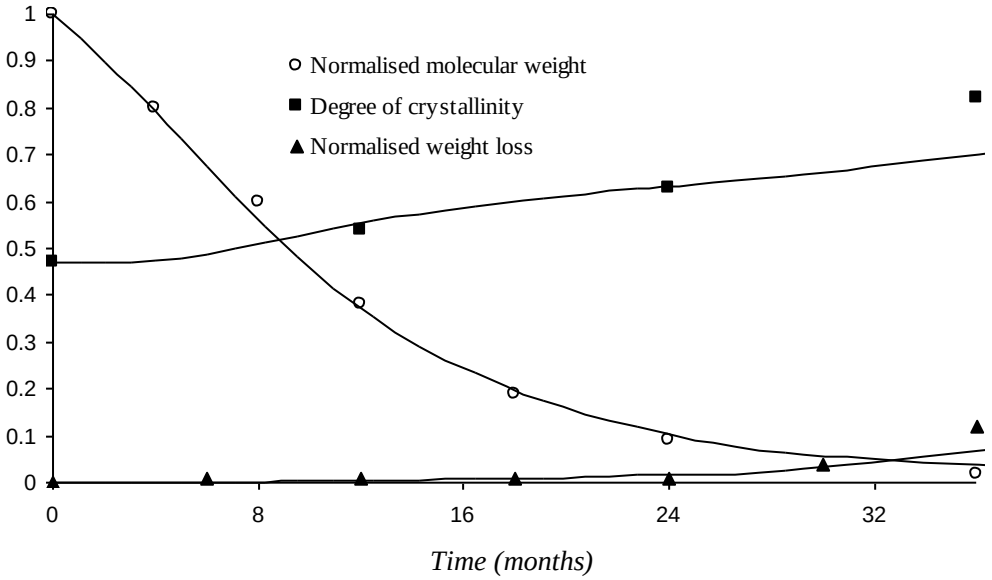

(b) $X_{c0} = 47\%$

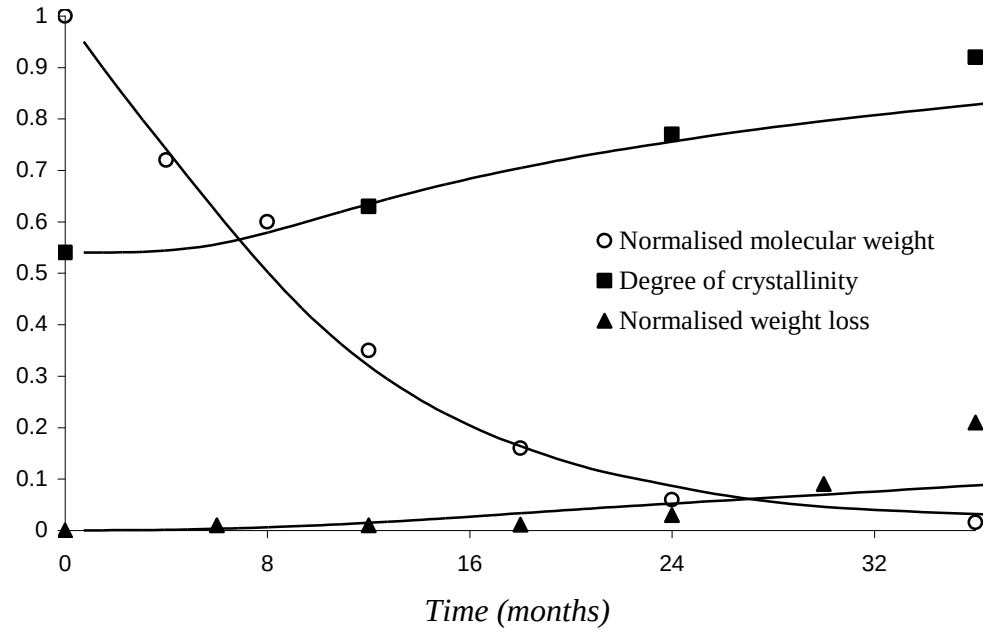

(c) $X_{c0} = 53\%$

Fig. 3. Comparison between the model and the experimental data obtained by Tsuji and Ikada [9] for PLLA films of different initial degree of crystallinity, showing average molecular weight, volume degree of crystallinity, and weight loss as functions of time. The continuous lines represent the model prediction while the discrete symbols are the experimental data by Tsuji and Ikada. The parameters used in the model are given in Table 1.

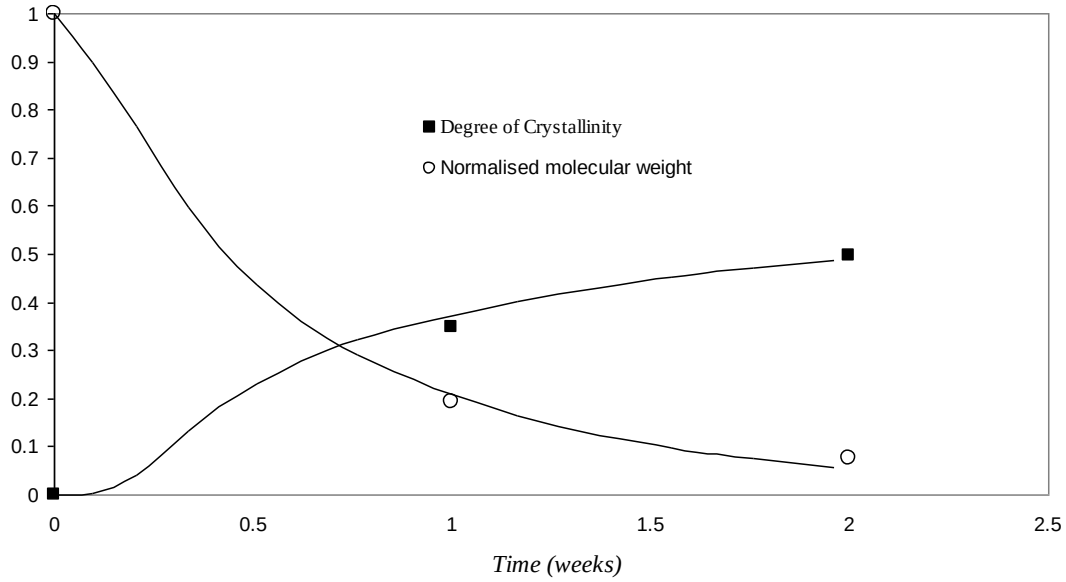

Fig. 4. Comparison between the model and the experimental data obtained by Zong et al. [7] for poly(glycolide-*co*-lactide), showing average molecular weight and volume degree of crystallinity as functions of time. The continuous lines represent the model prediction while the discrete symbols are the experimental data by Zong et al. [7]. The parameters used in the model are given in Table 1.

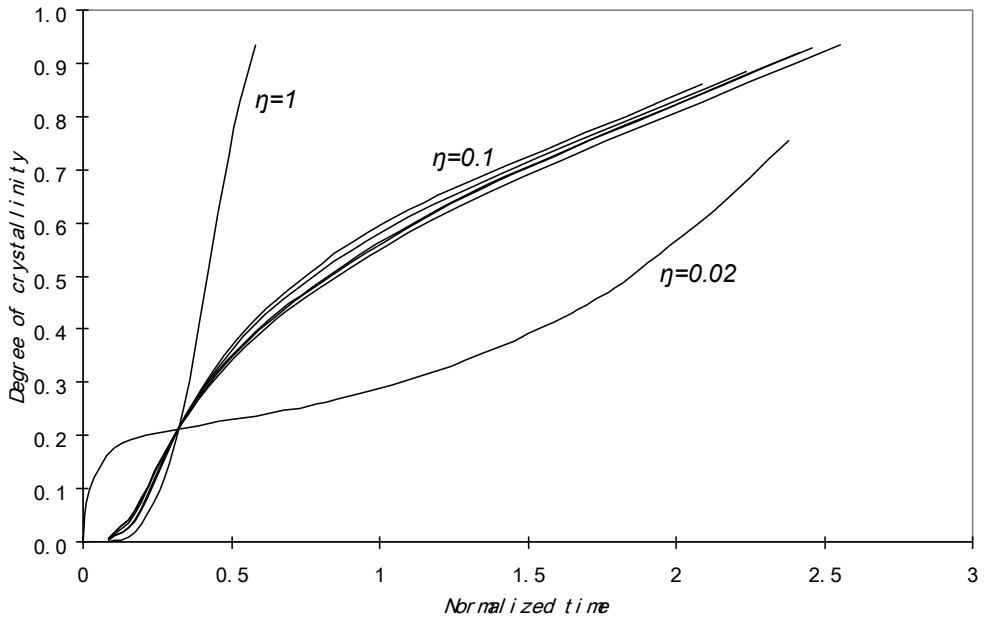

Fig 5. Effect of the five parameters in the crystallisation model on the degree of crystallinity as a function of time for a fixed value of $X_c = 0.2$ at $\overline{C}_e = 0.5$. For all the curves $\overline{D}_0 = 0.02$, $\overline{k}_1 = 1$ and $\overline{r}_{\max} = 4\pi/3\times10^4$. For the curve of $\eta = 1$, the following parameters were used: $\overline{N}_0 = 1$; $\overline{G} = 0.129$; $\overline{\xi} = 1000$. For the curve of $\eta = 0.02$, the following parameters were used: $\overline{N}_0 = 1$; $\overline{G} = 4.7$; $\overline{\xi} = 1000$. For the curve of $\eta = 0.1$, the following range of parameters were used: $\overline{N}_0 = 0.1$ to 1; $\overline{G} = 0.2$ to 10; $\overline{\xi} = 0.0013$ to 1000.

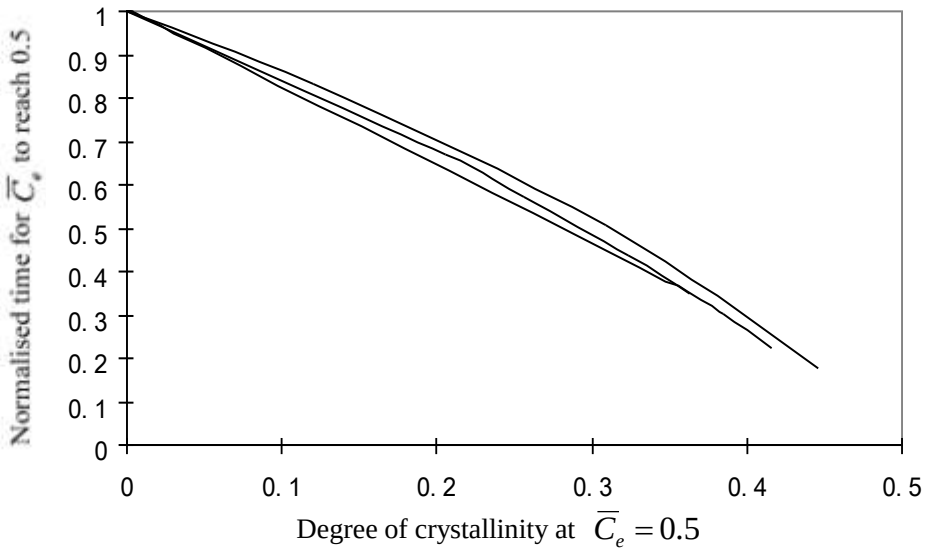

Fig. 6. Effect of crystallisation rate on the apparent hydrolysis rate showing fast crystallisation leads to fast apparent hydrolysis. $\bar{k}_1$=1, 100, 1000 for the three curves respectively; $\overline{D}_0 = 0.02$.

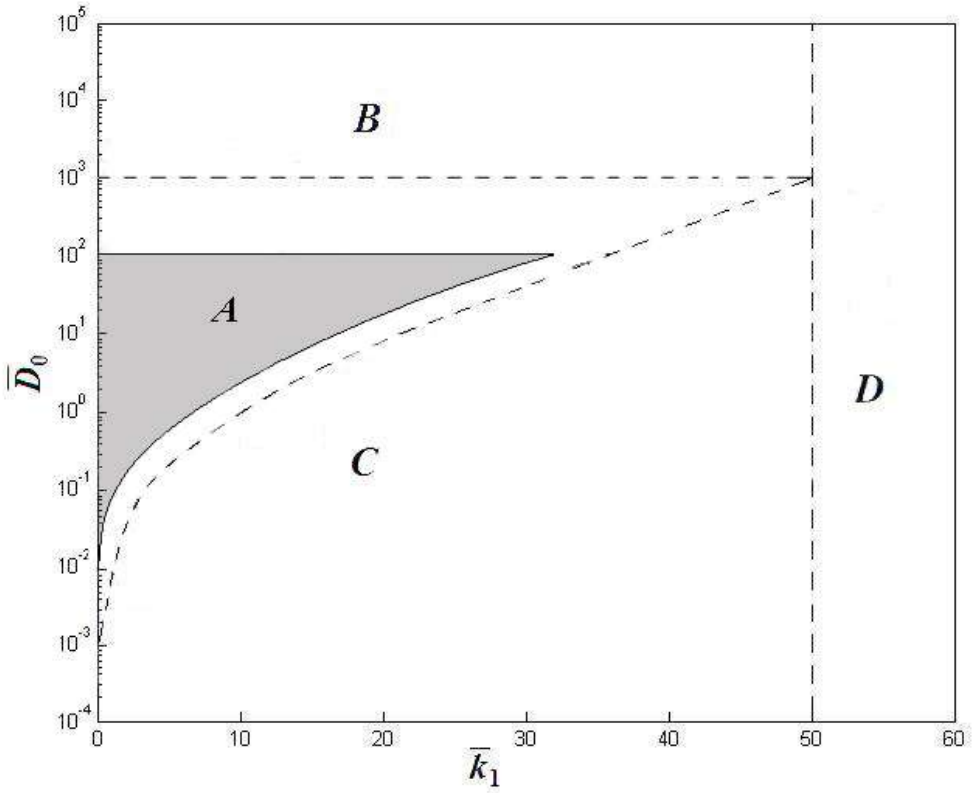

Fig. 7. Biodegradation map for infinitively large plate showing the controlling mechanism for biodegradation in the landscape of $\overline{D}_0$ and $\overline{k}_1$. The dash lines show the boundaries between the different zones for amorphous polymers. The shaded area is the newly calculated zone A for semi-crystalline polymers.